ACS Photonics

Article

pubs.acs.org/journal/apchd5

All-Dielectric Metasurfaces Based on Cross-Shaped Resonators for Color Pixels with Extended Gamut

Vishal Vashistha,*[,†,∥] Gayatri Vaidya,[‡,∥] Ravi S. Hegde,[§] Andriy E Serebryannikov,[†] Nicolas Bonod,[⊥] and Maciej Krawczyk*[,†]

[†]Faculty of Physics, Adam Mickiewicz University in Poznan, Poznan, Poland

[‡]Centre of Excellence in Nanoelectronics - CEN, IIT Bombay, Mumbai, India 400076

[§]Indian Institute of Technology, Gandhinagar, India 382355

[⊥]Aix Marseille University, CNRS, Centrale Marseille, Institut Fresnel, 13013 Marseille, France

Supporting Information

ABSTRACT: Printing technology based on plasmonic structures has many advantages over pigment-based color printing such as high resolution, ultracompact size, and low power consumption. However, due to high losses and broad resonance behavior of metals in the visible spectrum, it becomes challenging to produce well-defined colors. Here, we investigate cross-shaped dielectric nanoresonators, which enable high-quality resonances in the visible spectral regime and, hence, high-quality colors. We numerically predict and experimentally demonstrate that the proposed all-dielectric nanostructures exhibit high-quality colors with selective wavelengths, in particular, due to lower losses as compared to metal-based plasmonic filters. This results in fundamental colors (RGB) with high hue and saturation. We further show that a large gamut of colors can be achieved by selecting the appropriate length and width of individual Si nanoantennas. Moreover, the proposed all-dielectric metasurface-based color filters can be integrated with the well-matured fabrication technology of electronic devices.

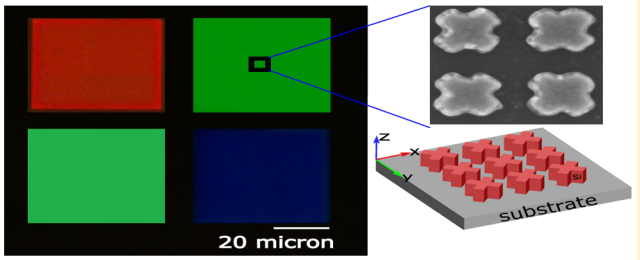

KEYWORDS: *all-dielectric nanophotonics, color filter, plasmonics, structural colors, nanoantenna*

With tremendous changes in nanotechnology over the past few decades, it becomes possible to fabricate devices that promise to revolutionize many areas. Examples include ultrathin planar lenses,[1,2] optical sensing,[3,4] photovoltaic devices,[5,6] nonfading colors,[7] and various holography-based devices.[8,9] In particular, color pixels using nanoparticles have gained significant attention in recent years because of several advantages over pigment-based color printing techniques such as high resolution,[10] high contrast, everlasting colors, significant low power consumption, and recyclability of products.[11] The concept of structural color printing is inspired by observations in nature, such as morpho butterflies, beetles, and the feathers of peacocks.[12−15] However, these colors are highly sensitive to the variations in the angle of incidence, shape, and size of the nanostructure. To make this plasmonics-based structural technology more mature, its angle dependency,[16,17] sensitivity to polarization, and ease of fabrication must be taken into account. In recent years, many efforts have been done to study the aforementioned issue in plasmonic color printing.[18−26] Earlier, the most commonly used materials for plasmonic nanostructure-based pixels have been gold and silver.[27,28] Gold has an interband transition in the lower visible regime,[27] while silver is suitable for the entire visible range but is susceptible to the native oxide, which spoils the stability of colors. Moreover, gold and silver are not economical for large-scale integration. Aluminum is probably the most prominent candidate.[29] It is more robust and economical for large-scale fabrication.[7] However, it shows lower quality (i.e., broader) resonance in the visible spectrum than gold or silver, especially at 800 nm wavelength, where interband transition takes place. Ultimately, all these metal-based plasmonic devices show significant losses within the visible spectrum.

On the other hand, all-dielectric metasurfaces can be a promising solution with significant advantages over metallic nanostructures such as high-quality resonances and low intrinsic ohmic losses.[30−38] Silicon-based all-dielectric devices have been reported for local manipulation by wavefronts, such as beam diversion, vortex plates, and light focusing using metalenses.[33,39−42] The advantages of Si nanodisks are high refractive index and ease of fabrication with well-established CMOS technology. Interestingly, the high refractive index allows manipulation by magnetic and electric components of light simultaneously. In the case of metal-based nanoantennas, absorption losses can be significant in the visible spectrum, while interaction with a magnetic component of the incident

Received: October 31, 2016
Published: March 30, 2017

© 2017 American Chemical Society

DOI: 10.1021/acsphotonics.6b00853
ACS Photonics 2017, 4, 1076−1082

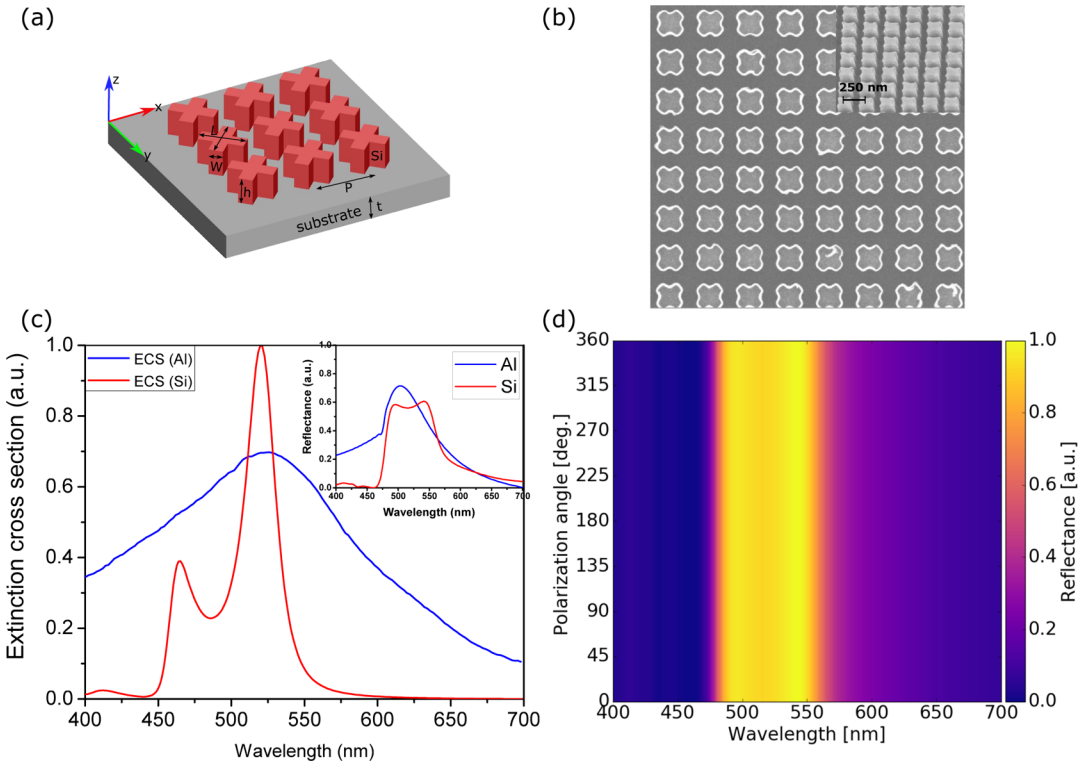

Figure 1. Perspective view and SEM images of the all-dielectric metasurface, extinction cross section (ECS) spectra, and reflectance spectra, and reflectance vs polarization angle. (a) Schematic representation of the array of cross-shaped Si nanoresonators on top of the quartz substrate. The thickness of the substrate is t = 275 μm. For each nanoantenna, height h = 140 nm and length L and width W are scaled to achieve different colors. The center-to-center distance between the two nanoresonators (lattice constant) is P = 250 nm. (b) Top view of SEM images of the fabricated structure with P = 250 nm. A 45° cross section view is added in the inset. (c) ECS spectra in the case of Si and Al nanoantennae. Two peaks arising in the former case are due to electric-type and magnetic-type resonance (see Supporting Information for the field patterns), while there is only a single broad resonance in the latter case. The inset shows the reflectance spectra for the same two structures. The length, width, and height are 100, 50, and 140 nm, respectively. (d) Colormap of simulated reflectance of the Si-based metasurface at a polarization angle varied from 0° to 360°.

beam requires more complex shapes. Recently, an investigation has been conducted to demonstrate the possibility of using silicon−aluminum hybrid nanodisks[43,44] to create colors of high quality. Silicon nanoparticles were proposed as a valuable alternative to plasmonic nanoantennae for the design of color pixels.[38,45−47] However, the potential of all-dielectric resonance structures is presently very far from being fully estimated and exploited.

In this work, we propose a systematic approach to build color filters by using advantages of cross-shaped Si nanoresonators, which are closely spaced to each other to create a metasurface. Recently reported numerical studies of the nanocross geometry[38] have indicated that a broader gamut of colors is possible in comparison to simpler shapes such as the cylinder (disk). The main goal is to obtain a high-quality (narrow) resonance throughout the visible spectrum that enables an extended gamut with colors of high purity. It is known that Si nanostructures of different shapes typically offer an opportunity to excite individual electric-type and magnetic-type Mie resonances or both resonances simultaneously.[48] In fact, it has been demonstrated that by tuning the aspect ratio carefully, one can overlap both resonances to achieve near-unity transmission.[40] In this paper, the all-dielectric metasurfaces are used in reflection mode. A very confined energy is concentrated within the structure due to the high quality of the used Mie resonances.

The main hypothesis that we follow here is based on the expectation that a proper manipulation by the selected Mie resonances may enable desired improvements of the resulting resonance quality owing to better confinement of resonance fields and, simultaneously, removal of secondary (unwanted) spectral features, so that enrichment of colors can be achieved. We decided in favor of cross-shaped Si nanoresonators as building elements, which are expected to be suitable[38] for achievement of the goals of this study. Each of them is made of two identical orthogonal rectangle-shaped Si nanoantennas. In this case, resonances are governed by cross-shaped nanoantennas, and thus, colors can be controlled via all three geometrical parameters of individual nanoantennas. This gives a new degree of freedom as compared to the nanodisks, which is highly demanded for efficient optimization. Using the suggested approach, we predict by simulations and confirm experimentally that one can easily achieve a high-quality resonance for the entire visible spectrum by carefully choosing the length and width of the cross-shaped nanoresonators.

RESULTS

Let us start from the general geometry and basic operation principles of the proposed devices. Figure 1a presents the perspective view of the proposed all-dielectric metasurface together with some details of geometry. The cross-shaped Si nanoresonators are deposited on top of the quartz substrate (see Methods of fabrication). The height of nanoantennae is selected as 140 nm (in subwavelength range). Figure 1b represents the top view of the SEM image of the device. A 45° cross section view is also added in the inset for the same

DOI: 10.1021/acsphotonics.6b00853
ACS Photonics 2017, 4, 1076−1082

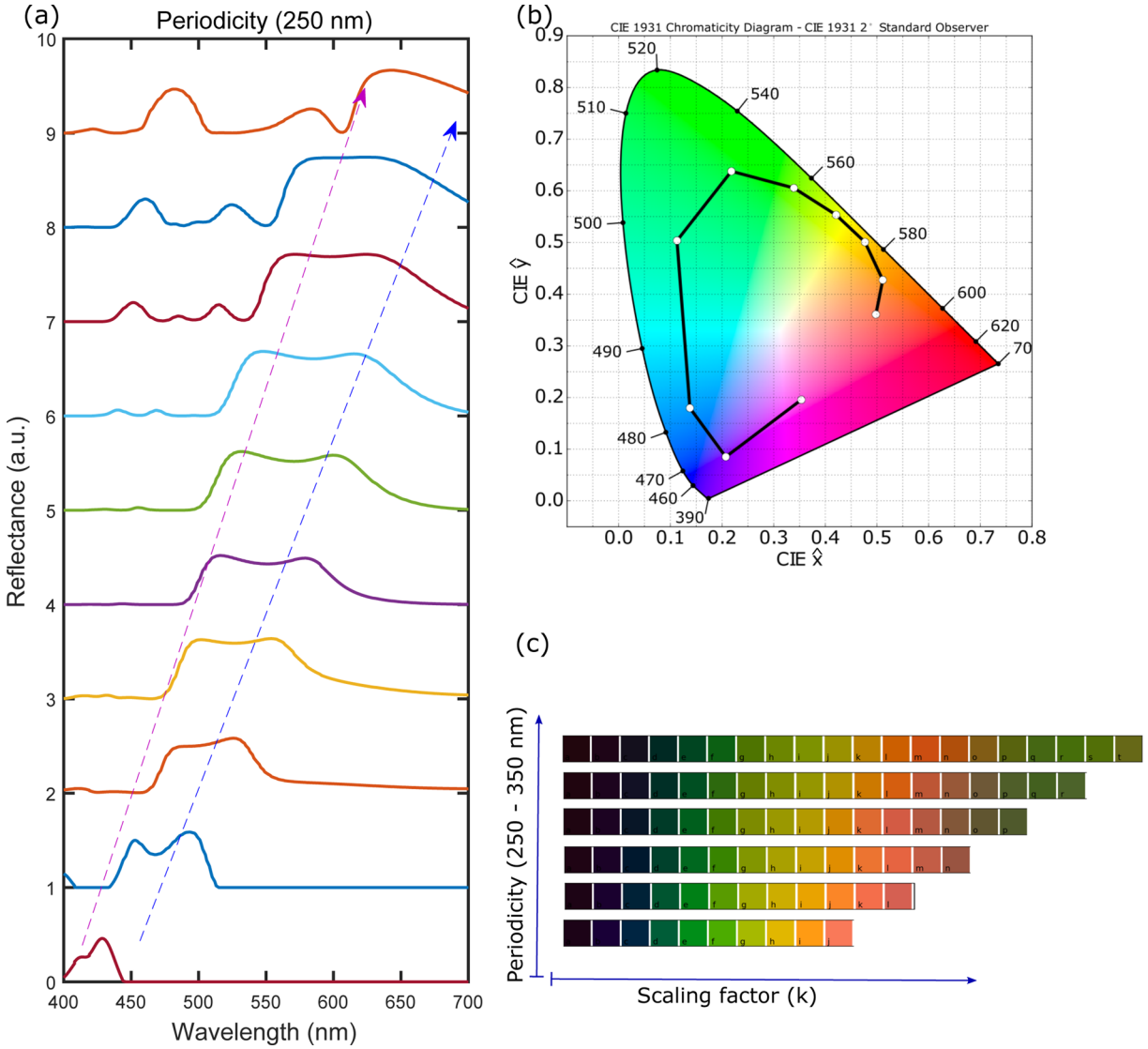

Figure 2. Reflectance spectra (simulation), corresponding chromaticity diagram, and photograph of experimental images of the array visible under an optical microscope. (a) Unit-cell simulation results for cross-shaped Si nanoresonators on a quartz substrate; the initial values of geometrical parameters are L = 65 nm, W = 35 nm, and P = 250 nm. L and W are linearly scaled from 65 nm to 195 nm and 35 nm to 105 nm, respectively, from bottom to top. The resonances are red-shifted in the visible regime, as schematically shown by arrows. (b) Representation of reflectance spectra on a standard CIE 1931 chromaticity diagram for P = 250 nm. (c) Experimental colors visible under an optical microscope for different values of P that are varied from 250 nm (the lowest series) to 350 nm (the most upper series) with steps of 20 nm (from the lowest series to the most upper one); L and W are linearly scaled from 65 nm to 260 nm and 35 nm to 140 nm, respectively, with $K = L/\min(L) = W/\min(W)$.

fabricated device. For the studied Si structure, the extinction cross section spectrum is presented in Figure 1c. Two resonance peaks are observed at 465 and 520 nm. They can be tuned throughout the visible range by changing the length-to-width aspect ratio of individual rectangle-shaped nano-antennas. The Si nanoresonator dimensions have been optimized to excite these two resonances as close as possible but without a full overlapping. In addition, the criterium of minimizing unwanted spectral features has been applied in order to obtain more gradual behavior in the working spectral range. As follows from the obtained simulation results, optimization yields a resonance range that is narrower and, thus, corresponds to a resonance of higher quality, as compared to the case of Al cross-shaped nanoantennae; see Figure 1c. We have also compared the simulated reflectance spectra for the metal- and Si-based structures at the same dimensions (see Figure 1c, inset). These results confirm that the metal nanostructure features broader resonances than the engineered Si one. An important advantage of cross-shaped nanoantennae is that they preserve the polarization independence. As an example, Figure 1d presents the simulated reflectance for the entire range of polarization angle variation and entire wavelength range considered. The obtained results confirm that there is no change in the reflectance when the polarization angle is varied.

Since a specific color results from resonant interaction of light with nanoresonators, it can be obtained from adjustment of geometrical parameters that properly affect spectral locations and properties of Mie resonances. The possibility of obtaining multiple colors with the aid of metasurfaces like that in Figure 1a and b is demonstrated in Figure 2. The length and width of rectangle-shaped Si nanoantennae are simultaneously linearly scaled in order to tune the electric- and magnetic-type resonances in the entire visible spectrum from 400 to 700

DOI: 10.1021/acsphotonics.6b00853
ACS Photonics 2017, 4, 1076−1082

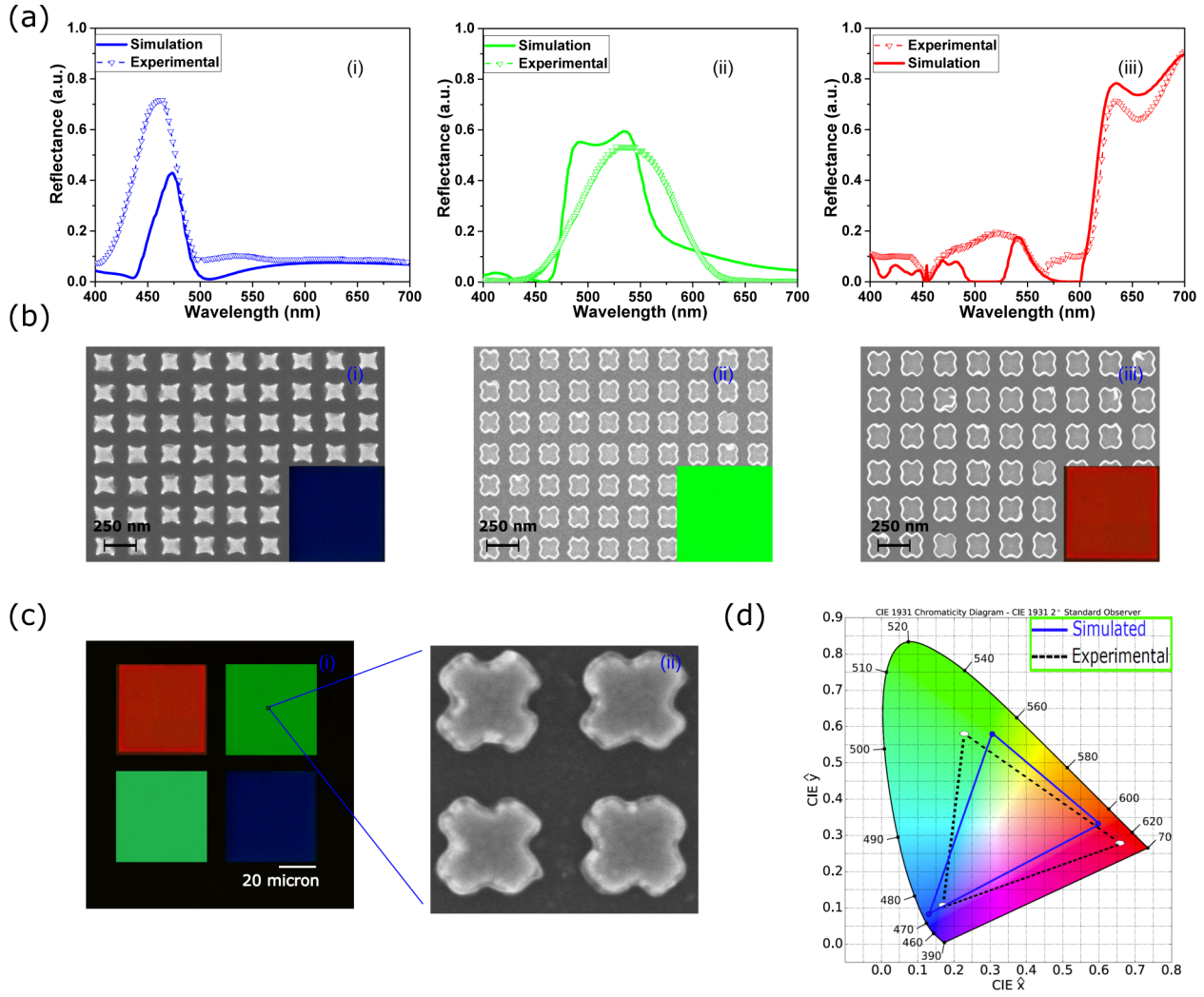

Figure 3. Simulation and experimental results for primary colors with SEM images. (a) Simulated and experimental reflectance spectra. The dimensions of cross-shaped Si nanoresonators: (i) L = 85 nm and W = 46 nm for blue color, (ii) L = 114 nm and W = 62 nm for green color, and (iii) L = 215 nm and W = 116 nm for red color. The lattice constant is 250 nm for all three cases. (b) SEM images of the fabricated structures with the inset view of associated colors. (c) Photograph taken with a Nikon camera attached with a 50× lens with NA = 0.65 and the enlarged SEM image of the nanostructure. (d) CIE 1931 chromaticity diagram that is used to visualize the simulated and measured colors.

nm, as shown in Figure 2a for P = 250 nm. A commercial-grade simulator based on the finite-difference time-domain method[49] is used to perform the calculations. They are conducted for a unit cell with periodic boundary conditions and varied lattice constants from 250 to 350 nm, by keeping the periodicity in the subwavelength range (see Methods, Simulation). Each spectral zone in Figure 2a corresponds to a specific color. It is clearly seen that the electric- and magnetic-type resonances can be tuned through the entire visible wavelength spectrum, as desired. Conversion of reflectance spectra into colors on a CIE1931 chromaticity diagram can be performed, in the general case, by using an open source Python program.[50] The results of conversion of the spectra shown in Figure 2a are presented in Figure 2b. Generally, a higher quality of resonances corresponds to a better approach to the boundaries of the chromaticity diagram and, hence, enable higher quality and a wider gamut of colors. Complete details about color visualization using reflectance spectra are given in the Supporting Information under the section color representation from reflectance spectra.

By operating the metasurface in reflection mode, a broad spectrum of colors for highly selective wavelengths (i.e., high-quality colors) can be obtained. In principle, colors can be generated by using either an additive or subtractive approach.[51] Here, we have used the additive approach. Ideally, the reflection spectrum must be as narrow as possible in order to generate a very specific color. A narrower resonance represents a more specific wavelength color, whereas the amplitude of the peak decides the saturation level of the color. With the aid of high-quality (narrow) resonances, we improve the approach to the boundaries of the CIE-1931 chromaticity diagram, so a color of higher quality and a wider gamut of colors can be obtained, as desired. We experimentally found that different colors can be obtained at different values of the period (P, lattice constant), which corresponds to the scaled length (L) and width (W) of the nanoantenna; see Figure 2c. Each square in Figure 2c corresponds to a unique set of geometrical parameters. The lowest series of the squares shown here corresponds to the structures for which reflectance spectra are presented in Figure 2a. Thus, the resonance region corresponds to different colors at different values of P; see Figure S4 in the Supporting

DOI: 10.1021/acsphotonics.6b00853
ACS Photonics 2017, 4, 1076−1082

Information. This dependence occurs owing to the coupling of resonance fields of nanoresonators. The use of larger values of P allows us to create a richer variety of colors, as we have more choices to increase the length and width. We have observed different colors under an optical microscope due to variations in lattice constant (P) from 250 to 350 nm; see Figure 2c. The lattice constant was increased here by a reasonable increment of 20 nm to make it feasible for the fabrication process. Although it might be hard to distinguish between the highly saturated colors in Figure 2c, the reflectance spectra in Figure 2a and the corresponding CIE-1931 chromaticity diagram in Figure 2b give us a clear picture about it. In fact, a color gamut can be possible by making a matrix between the scaled lengths and widths.

The fact that two resonances, which are observed in Figure 2a at different values of L and W, are closely spaced makes fabrication of a particular color possible, which is unlikely in the case of metal-based plasmonic structures, because they show a broad resonance. Moreover, it is possible to create a selective wavelength color due to sharp resonances, particularly in the lower part of the visible spectrum. It is observed in Figure 2a that as we increase the size of cross-shaped resonators, some additional Mie resonances are also excited, in coincidence with the predictions based on the simulation results. These resonances reduce the hue and saturation of red color, because of the mixing contribution of different frequencies. So the red color seems to be the most difficult one to fabricate. Below, we will show that in spite of the above-mentioned difficulties the suggested structure allows us creating fairly red colors by carefully adjusting the values of P, L, and W. Thanks to this adjustment, the unwanted effect of higher order resonances can be minimized.

The three primary colors (RGB) represent the fundamental unit for color printing technology. All the other colors in the RGB gamut can be derived by mixing the primary colors appropriately. Figure 3 presents the results of a detailed experimental demonstration of the suggested devices in the form of pixels. A dual characterization is done to ensure the results by measuring the reflectance spectra of the samples with the aid of a homemade customized setup and observing the colors directly under an optical microscope (see Methods, Optical Characterization). Figure 3a shows the experimental and simulated reflectance spectra for highly saturated primary colors. These results show good agreement with each other. Figure 3b shows the SEM images obtained at different sizes of nanoantennas. Insets are added to the SEM images to show the corresponding colors visible under an optical microscope, which are associated with the different sizes of the cross-shaped nanoresonators. Finally, these three primary colors are fabricated in the form of a pixel, being the main component of any display device. The size of each square block is 50 μm. Details of the used fabrication method are given at the end of the paper. The optical microscope images shown in Figure 3c confirm the quality of highly saturated primary colors, which is an important advantage of the suggested all-dielectric metasurface-based pixels over the existing plasmonic devices. A CIE 1931 chart is used to represent the simulated and experimental spectra of the primary colors; see Figure 3d. One can see a very small shift in the color spectrum, which might come from fabrication imperfections. It is noticeable that there is good coincidence between the two sets of experimental results.

CONCLUSION

Polarization-insensitive all-dielectric metasurfaces based on 2D arrays of cross-shaped Si nanoresonators have been proposed to realize color filters with extended gamut for the entire visible spectrum. A numerical investigation has been carried out that demonstrates the principal possibility of obtaining high-purity colors by means of optimization of resonance properties, which can be realized by a relatively simple adjustment of the structural parameters. The role of existence and properties of the dual resonance, which is achieved at a partial overlapping of electric-type and magnetic-type resonances and that of suppression of unwanted spectral features in the obtaining of these advancements have been clarified. The utilized resonances can be tuned by changing the length-to-width aspect ratio of individual rectangle-shaped nanoantennas. This concept has been used to design and fabricate the color filters. Our simulation results reasonably agree with the experimental ones. Some differences should be noticed that may be connected with fabrication complexity of the structure. The experimentally demonstrated possibility of obtaining high-quality (narrow) resonances, which enable high-quality colors, is the most important result of this work. We have demonstrated the wide variety of colors for different periodicity and size of cross-shaped nanoresonators. Additionally, we have demonstrated the primary color painting in the form of pixels. These colors show high saturation and hue value. In fact, our device is able to produce a large panel of colors in the visible regime with strong spectral selectivity, provided that the nanoantenna aspect ratio is properly chosen. By carefully controlling the balance between desired and unwanted Mie resonances, one can further optimize the color filter, especially in the dark zone of red color. Since a-Si (amorphous-*Si*) is the most suitable material for large-scale fabrication with the existing technology, it can potentially be used for making low-cost, eco-friendly, high-quality, long-lasting painting possible for mass production in the future.

METHODS

Simulations. We have used Lumerical FDTD solver[49] to study metasurfaces comprising the cross-shaped nanoresonators on a dielectric substrate. The materials used for substrate and cross-shaped nanoresonators are SiO_2 and Si, respectively. The material parameters are taken from the default material library of the used software. A plane wave ranging from 400 to 700 nm is incident from the top of the structure. Periodic boundary conditions are used in the unit cell along the x and y directions. Perfect matching layer boundary conditions were used in the z direction to avoid any reflection. The reflectance spectra are simulated by considering a unit cell (one cross-shaped nanoresonator on a substrate) with periodic boundary conditions in the x and y directions.

Device Fabrication. A piranha-cleaned quartz sample (275 μm thick) is used to fabricate the device. We have deposited a thin layer of 140 nm amorphous Si using the ICPCVD tool at 300 °C with 150 W added microwave power. A single-layer poly(methyl methacrylate) (PMMA) photoresist is used for patterning cross-shaped nanoresonators by using the Raith 150-Two EBL tool. An electronic mask is designed using an open source Python program. The exposed sample is developed using methyl isobutyl ketone−isopropyl alcohol (IPA) (1:3) and an IPA solution for 45 and 15 s, respectively. A thin layer of metal (5 nm of Cr as an adhesion layer and 40 nm of Au) is

DOI: 10.1021/acsphotonics.6b00853
ACS Photonics 2017, 4, 1076−1082

deposited to transfer the pattern on the metal layer for the lift-off process using four target evaporators. After lift-off, the sample is etched using plasma asher to get the final pattern. A process flowchart with step-by-step details is available in the Supporting Information.

Optical Characterization. A dual optical characterization is done to ensure the results. The sample is placed under an Olympus optical microscope and illuminated with white light without a filter. The colors can be directly seen under an optical microscope. The reflectance spectra are measured using a homemade customized setup. An HL 2000 halogen lamp source is coupled with an optical fiber to illuminate the sample in the visible range, i.e., from 400 to 700 nm. A 50× objective lens with NA = 0.65 is used to get a tight focusing of light on the sample. The reflectance spectra are measured using the same objective lens. All the collected data are normalized with respect to the bare quartz sample. A Nikon camera attached with the assembly is used to take the photograph of the illuminated area.

■ ASSOCIATED CONTENT

Supporting Information

The Supporting Information is available free of charge on the ACS Publications website at DOI: 10.1021/acsphotonics.6b00853.

Additional information (PDF)

■ AUTHOR INFORMATION

Corresponding Authors

*E-mail (V. Vashistha): visvas@amu.edu.pl.

*E-mail (M. Krawczyk): krawczyk@amu.edu.pl.

ORCID

Vishal Vashistha: 0000-0003-4174-6709

Author Contributions

‖V. Vashistha and G. Vaidya contributed equally to this work.

Notes

The authors declare no competing financial interest.

■ ACKNOWLEDGMENTS

R.S.H. acknowledges support from the Department of Science and Technology, India, under the Extramural Research Grant No. SB/S3/EECE/0200/2015. R.S.H., V.V., and G.V. acknowledge support from the Indian Nanoelectronics Users Program under Grant Nos. P643987963 and P875860276. The work was partially supported by the National Science Centre Poland for OPUS Grant No. 2015/17/B/ST3/00118(Metasel) and by the European Union Horizon2020 research and innovation program under the Marie Sklodowska-Curie grant agreement No. 644348 (MagIC). The authors thank all the members of the CEN laboratory, IIT Bombay, who helped us directly or indirectly while doing nanofabrication work. Special thanks to Dr. K Nageshwari and Dr. Ritu Rashmi for providing necessary facilities and regular advice.

■ REFERENCES

(1) Kildishev, A. V.; Boltasseva, A.; Shalaev, V. M. Planar photonics with metasurfaces. *Science* **2013**, *339*, 1232009.

(2) Yu, N.; Capasso, F. Flat optics with designer metasurfaces. *Nat. Mater.* **2014**, *13*, 139−150.

(3) Adato, R.; Yanik, A. A.; Amsden, J. J.; Kaplan, D. L.; Omenetto, F. G.; Hong, M. K.; Erramilli, S.; Altug, H. Ultra-sensitive vibrational spectroscopy of protein monolayers with plasmonic nanoantenna arrays. *Proc. Natl. Acad. Sci. U. S. A.* **2009**, *106*, 19227−19232.

(4) Liu, N.; Mesch, M.; Weiss, T.; Hentschel, M.; Giessen, H. Infrared perfect absorber and its application as plasmonic sensor. *Nano Lett.* **2010**, *10*, 2342−2348.

(5) Atwater, H. A.; Polman, A. Plasmonics for improved photovoltaic devices. *Nat. Mater.* **2010**, *9*, 205−213.

(6) Chen, X.; Jia, B.; Saha, J. K.; Cai, B.; Stokes, N.; Qiao, Q.; Wang, Y.; Shi, Z.; Gu, M. Broadband enhancement in thin-film amorphous silicon solar cells enabled by nucleated silver nanoparticles. *Nano Lett.* **2012**, *12*, 2187−2192.

(7) James, T. D.; Mulvaney, P.; Roberts, A. The plasmonic pixel: large area, wide gamut color reproduction using aluminum nanostructures. *Nano Lett.* **2016**, *16*, 3817−3823.

(8) Almeida, E.; Bitton, O.; Prior, Y. Nonlinear metamaterials for holography. *Nat. Commun.* **2016**, *7*, 12533.

(9) Ni, X.; Kildishev, A. V.; Shalaev, V. M. Metasurface holograms for visible light. *Nat. Commun.* **2013**, *4*, 3807.

(10) Tan, S. J.; Zhang, L.; Zhu, D.; Goh, X. M.; Wang, Y. M.; Kumar, K.; Qiu, C.-W.; Yang, J. K. Plasmonic color palettes for photorealistic printing with aluminum nanostructures. *Nano Lett.* **2014**, *14*, 4023−4029.

(11) Clausen, J. S.; Højlund-Nielsen, E.; Christiansen, A. B.; Yazdi, S.; Grajower, M.; Taha, H.; Levy, U.; Kristensen, A.; Mortensen, N. A. Plasmonic metasurfaces for coloration of plastic consumer products. *Nano Lett.* **2014**, *14*, 4499−4504.

(12) Srinivasarao, M. Nano-optics in the biological world: beetles, butterflies, birds, and moths. *Chem. Rev.* **1999**, *99*, 1935−1962.

(13) Vukusic, P.; Sambles, J.; Lawrence, C.; Wootton, R. Structural colour: now you see it —now you don't. *Nature* **2001**, *410*, 36−36.

(14) Kinoshita, S.; Yoshioka, S.; Miyazaki, J. Physics of structural colors. *Rep. Prog. Phys.* **2008**, *71*, 076401.

(15) Gralak, B.; Tayeb, G.; Enoch, S. Morpho butterflies wings color modeled with lamellar grating theory. *Opt. Express* **2001**, *9*, 567−578.

(16) Wu, Y.-K. R.; Hollowell, A. E.; Zhang, C.; Guo, L. J. Angle-insensitive structural colours based on metallic nanocavities and coloured pixels beyond the diffraction limit. *Sci. Rep.* **2013**, *3*, 1194.

(17) Højlund-Nielsen, E.; Weirich, J.; Nørregaard, J.; Garnaes, J.; Mortensen, N. A.; Kristensen, A. Angle-independent structural colors of silicon. *J. Nanophotonics* **2014**, *8*, 083988−083988.

(18) Kumar, K.; Duan, H.; Hegde, R. S.; Koh, S. C.; Wei, J. N.; Yang, J. K. Printing colour at the optical diffraction limit. *Nat. Nanotechnol.* **2012**, *7*, 557−561.

(19) Roberts, A. S.; Pors, A.; Albrektsen, O.; Bozhevolnyi, S. I. Subwavelength plasmonic color printing protected for ambient use. *Nano Lett.* **2014**, *14*, 783−787.

(20) Ellenbogen, T.; Seo, K.; Crozier, K. B. Chromatic plasmonic polarizers for active visible color filtering and polarimetry. *Nano Lett.* **2012**, *12*, 1026−1031.

(21) Diest, K.; Liberman, V.; Lennon, D. M.; Welander, P. B.; Rothschild, M. Aluminum plasmonics: optimization of plasmonic properties using liquid-prism-coupled ellipsometry. *Opt. Express* **2013**, *21*, 28638−28650.

(22) Li, Z.; Clark, A. W.; Cooper, J. M. Dual color plasmonic pixels create a polarization controlled nano color palette. *ACS Nano* **2016**, *10*, 492−498.

(23) Duempelmann, L.; Casari, D.; Luu-Dinh, A.; Gallinet, B.; Novotny, L. Color rendering plasmonic aluminum substrates with angular symmetry breaking. *ACS Nano* **2015**, *9*, 12383−12391.

(24) Wang, L.; Ng, R. J. H.; Safari Dinachali, S.; Jalali, M.; Yu, Y.; Yang, J. K. Large area plasmonic color palettes with expanded gamut using colloidal self-assembly. *ACS Photonics* **2016**, *3*, 627−633.

(25) Richner, P.; Galliker, P.; Lendenmann, T.; Kress, S. J.; Kim, D. K.; Norris, D. J.; Poulikakos, D. Full-spectrum flexible color printing at the diffraction limit. *ACS Photonics* **2016**, *3*, 754−757.

(26) Fan, J.; Wu, W.; Chen, Z.; Zhu, J.; Li, J. Three-dimensional cavity nanoantennas with resonant-enhanced surface plasmons as dynamic color-tuning reflectors. *Nanoscale* **2017**,.9341610.1039/C6NR06934G

DOI: 10.1021/acsphotonics.6b00853
ACS Photonics 2017, 4, 1076−1082

(27) Ehrenreich, H.; Philipp, H. R. Optical properties of Ag and Cu. *Phys. Rev.* **1962**, *128*, 1622−1629.
(28) West, P. R.; Ishii, S.; Naik, G. V.; Emani, N. K.; Shalaev, V. M.; Boltasseva, A. Searching for better plasmonic materials. *Laser & Photonics Rev.* **2010**, *4*, 795−808.
(29) Gérard, D.; Gray, S. K. Aluminium plasmonics. *J. Phys. D: Appl. Phys.* **2015**, *48*, 184001.
(30) Paniagua-Domínguez, R.; Yu, Y. F.; Miroschnichenko, A. E.; Krivitsky, L. A.; Fu, Y. H.; Valuckas, V.; Gonzaga, L.; Toh, Y. T.; Kay, A. Y. S.; Luk'yanchuk, B.; Kuznetsov, A. I. Generalized Brewster effect in dielectric metasurfaces. *Nat. Commun.* **2016**, *7*, 10362.
(31) Bonod, N. Silicon photonics: Large-scale dielectric metasurfaces. *Nat. Mater.* **2015**, *14*, 664−665.
(32) Jahani, S.; Jacob, Z. All-dielectric metamaterials. *Nat. Nanotechnol.* **2016**, *11*, 23−36.
(33) Decker, M.; Staude, I.; Falkner, M.; Dominguez, J.; Neshev, D. N.; Brener, I.; Pertsch, T.; Kivshar, Y. S. High-efficiency dielectric Huygens. *Adv. Opt. Mater.* **2015**, *3*, 813−820.
(34) Sautter, J.; Staude, I.; Decker, M.; Rusak, E.; Neshev, D. N.; Brener, I.; Kivshar, Y. S. Active tuning of all-dielectric metasurfaces. *ACS Nano* **2015**, *9*, 4308−4315.
(35) Li, J.; Verellen, N.; Vercruysse, D.; Bearda, T.; Lagae, L.; Van Dorpe, P. All-dielectric antenna wavelength router with bidirectional scattering of visible light. *Nano Lett.* **2016**, *16*, 4396−4403.
(36) Moitra, P.; Slovick, B. A.; Li, W.; Kravchencko, I. I.; Briggs, D. P.; Krishnamurthy, S.; Valentine, J. Large-scale all-dielectric metamaterial perfect reflectors. *ACS Photonics* **2015**, *2*, 692−698.
(37) Liu, S.; Sinclair, M. B.; Mahony, T. S.; Jun, Y. C.; Campione, S.; Ginn, J.; Bender, D. A.; Wendt, J. R.; Ihlefeld, J. F.; Clem, P. G.; Wright, J. B.; Brener, I. Optical magnetic mirrors without metals. *Optica* **2014**, *1*, 250−256.
(38) Hegde, R. S.; Panse, K. S. Design and optimization of ultrathin spectral filters based on silicon nanocross antenna arrays. *J. Nanophotonics* **2016**, *10*, 026030−026030.
(39) Shalaev, M. I.; Sun, J.; Tsukernik, A.; Pandey, A.; Nikolskiy, K.; Litchinitser, N. M. High-efficiency all-dielectric metasurfaces for ultracompact beam manipulation in transmission mode. *Nano Lett.* **2015**, *15*, 6261−6266.
(40) Staude, I.; Miroshnichenko, A. E.; Decker, M.; Fofang, N. T.; Liu, S.; Gonzales, E.; Dominguez, J.; Luk, T. S.; Neshev, D. N.; Brener, I.; Kivshar, Y. Tailoring directional scattering through magnetic and electric resonances in subwavelength silicon nanodisks. *ACS Nano* **2013**, *7*, 7824−7832.
(41) Lin, D.; Fan, P.; Hasman, E.; Brongersma, M. L. Dielectric gradient metasurface optical elements. *Science* **2014**, *345*, 298−302.
(42) Arbabi, A.; Horie, Y.; Bagheri, M.; Faraon, A. Dielectric metasurfaces for complete control of phase and polarization with subwavelength spatial resolution and high transmission. *Nat. Nanotechnol.* **2015**, *10*, 937−943.
(43) Yue, W.; Gao, S.; Lee, S.-S.; Kim, E.-S.; Choi, D.-Y. Subtractive color filters based on a silicon-aluminum hybrid-nanodisk metasurface enabling enhanced color purity. *Sci. Rep.* **2016**, *6*, 29756.
(44) Shrestha, V. R.; Lee, S.-S.; Kim, E.-S.; Choi, D.-Y. Polarization-tuned dynamic color filters incorporating a dielectric-loaded aluminum nanowire array. *Sci. Rep.* **2015**, *5*, 12450.
(45) Cao, L.; Fan, P.; Barnard, E. S.; Brown, A. M.; Brongersma, M. L. Tuning the color of silicon nanostructures. *Nano Lett.* **2010**, *10*, 2649−2654.
(46) Proust, J.; Bedu, F.; Gallas, B.; Ozerov, I.; Bonod, N. All-dielectric colored metasurfaces with silicon Mie resonators. *ACS Nano* **2016**, *10*, 7761−7767.
(47) Zhao, W.; Liu, B.; Jiang, H.; Song, J.; Pei, Y.; Jiang, Y. Full-color hologram using spatial multiplexing of dielectric metasurface. *Opt. Lett.* **2016**, *41*, 147−150.
(48) Kuznetsov, A. I.; Miroshnichenko, A. E.; Fu, Y. H.; Zhang, J.; Luk'yanchuk, B. Magnetic light. *Sci. Rep.* **2012**, *2*, 00492.
(49) http://www.lumerical.com/tcad-products/fdtd/.
(50) http://colour.readthedocs.io/en/latest.
(51) https://graphics.stanford.edu/courses/cs178/applets/custom-subtractive-too-wide.jpg.

DOI: 10.1021/acsphotonics.6b00853
ACS Photonics 2017, 4, 1076−1082